

Momentum Transport from Current-Driven Reconnection in the Reversed Field Pinch

F. Ebrahimi, V. V. Mirnov, S. C. Prager, and C. R. Sovinec

Center for Magnetic Self-Organization in Laboratory and Astrophysical Plasmas, and University of Wisconsin–Madison, Madison, Wisconsin 53706, USA

(Received 15 June 2006; published 16 August 2007)

We calculate momentum transport from tearing fluctuations in a reversed field pinch with sheared flow, considering both the effect of a single tearing mode (through quasilinear theory and MHD computation) and multiple tearing modes (through nonlinear MHD computation). A single tearing mode transports momentum, via Maxwell and Reynolds stresses, more rapidly than classical viscous forces. Moreover, the transport is enhanced by nonlinear coupling of multiple modes.

DOI: [10.1103/PhysRevLett.99.075003](https://doi.org/10.1103/PhysRevLett.99.075003)

PACS numbers: 52.30.Cv, 52.35.Vd, 52.65.Kj

Toroidal plasmas are often observed to rotate in the toroidal direction, in both astrophysical and laboratory settings. It is also observed in both venues that the toroidal angular momentum can be rapidly transported in the radial direction. For example, in accretion disks surrounding black holes, as particles fall radially in toward the black hole, angular momentum is transported radially outward. That is, such transport is needed to maintain a Keplerian rotation profile as individual particles gain momentum from inward motion. In the toroidal laboratory configuration of the reversed field pinch (RFP), rapid momentum transport occurs as a flattening of the radial profile of the toroidal rotation during a reconnection event [1]. In both cases, momentum transport is faster than can be explained by collisional viscosity. Also, for both cases the leading explanations of momentum transport are stresses (Maxwell and Reynolds) arising from MHD instabilities: a flow-driven instability for accretion disks (e.g., [2,3]) and a current-driven instability for the RFP.

In this Letter, we examine theoretically the laboratory example of momentum transport from current-driven reconnection, a process possibly also relevant to astrophysical plasmas. In the RFP, the dominant instabilities are resistive tearing modes, nonlinearly coupled to each other. Coupling between three tearing modes with different wave numbers can produce localized torques that transport momentum. This notion was introduced previously through analysis of the ideal MHD equations away from the resonant surfaces [4,5].

To elucidate the physics of the torques, we perform three sets of calculations, of increasing completeness. Each treats an RFP plasma with sub-Alfvénic flow. First, we examine torques arising from a single tearing mode in the linear regime. The torques are localized to the reconnection layer. We display the analytic solutions for the Maxwell and Reynolds stresses from quasilinear theory and from computational solution of the exact linearized equations. Linear theory provides the spatial structure of the stresses, which proves to be very similar to that in the nonlinear regime. Second, we compute the stresses for the full nonlinear evolution of a single tearing mode, which

yields a momentum transport rate 1000 times faster than that due to classical viscosity. Third, we compute the complete case of multiple, nonlinearly coupled tearing modes. Comparison to the single nonlinear mode reveals the important additional effects from nonlinear coupling. The torques are strengthened. The effect of multiple tearing modes is not merely the superposition of independent, radially separated effects. Rather, the torque arising from the stress of one spatial mode (among many) is itself increased by the presence of other modes. For example, the phase between the current density and magnetic field of a specific mode is altered (from the case of one mode only) so as to increase the Maxwell stress.

We first calculate the quasilinear torque arising from a single tearing mode. Linear tearing modes with equilibrium flows [6–8], including shear [9–13], have been studied previously in a slab. Here, we concentrate on the torque and employ a cylindrical plasma with equilibrium helical magnetic field (azimuthal and axial) and axial flow. The assumed flow $V_z(r)$ is weak, and only negligibly destabilizing due to its shear dV_z/dr [10,12]. We solve for the eigenfunctions in the resistive, reconnection layer (which is smaller than the island width) and in the ideal, outer regions, from which we construct the Lorentz force ($\tilde{\mathbf{J}} \times \tilde{\mathbf{B}}$, where tilde denotes perturbations) arising from the Maxwell stress and the fluid force arising from the Reynolds stress ($\rho \tilde{\mathbf{V}} \cdot \nabla \tilde{\mathbf{V}}$). For a force-free equilibrium with perturbations of the form $\tilde{a}(r) \exp(\gamma t + im\theta - ik_z z)$, the linearized resistive MHD equations are

$$\begin{aligned} \rho \gamma^2 \xi + \rho \gamma (\mathbf{V}_0 \cdot \nabla) \xi + \rho \gamma (\xi \cdot \nabla) \mathbf{V}_0 \\ = (\nabla \times \tilde{\mathbf{B}}) \times \mathbf{B} + \mathbf{J} \times \tilde{\mathbf{B}} - \nabla \tilde{p}, \\ \tilde{p} + 1/\gamma (\mathbf{V}_0 \cdot \nabla) \tilde{p} = -(\xi \cdot \nabla p) - \Gamma p \nabla \cdot \xi, \\ \tilde{\mathbf{B}} - \eta/\gamma \nabla^2 \tilde{\mathbf{B}} = \nabla \times (\xi \times \mathbf{B}) + 1/\gamma \nabla \times (\mathbf{V}_0 \times \tilde{\mathbf{B}}). \end{aligned} \quad (1)$$

We adopt tearing ordering [14] $\gamma \propto \eta^{3/5}$, $\gamma \rightarrow \epsilon^3$, $\eta \rightarrow \epsilon^5$, $(r - r_s) \rightarrow \epsilon^2 x$, where r_s denotes the resonant surface ($k_{\parallel} = 0$) and ϵ is a small parameter. We assume $g = \mathbf{k} \cdot \mathbf{V}_0 = -k_z V_z$ vanishes at $r = r_s$ and varies linearly with x in the inner region, $g = g'(r_s)x$. We consider a small

equilibrium flow of order $V_0 \approx \eta^{1/5}$ [$g = (k \cdot V_0)'_{(r_s)} x \rightarrow \epsilon^3$]. Expanding the displacement and magnetic field perturbations in powers of ϵ , as in [14], the inner layer equations for the magnetic field (radial and parallel), and the displacement with flow shear become

$$\frac{\eta}{\gamma} \tilde{B}_r^{(6)''} = \left(1 + \frac{ig'x}{\gamma}\right) \tilde{B}_r^{(4)} - (\mathbf{B} \cdot \nabla) \xi_r^{(2)} \quad (2)$$

$$\begin{aligned} \rho \gamma^2 \left(1 + \frac{ig'x}{\gamma}\right) \xi_r^{(2)''} = & \left[\frac{(\mathbf{B} \cdot \nabla) \gamma}{\eta} \left(1 + \frac{ig'x}{\gamma}\right) \right. \\ & \left. + ik_{\perp} \frac{(\mathbf{J} \cdot \mathbf{B})'}{B} \right] \tilde{B}_r^{(4)} \\ & - \frac{(\mathbf{B} \cdot \nabla)^2 \gamma}{\eta} \xi_r^{(2)} + \frac{2B_{\theta}^2 k_{\perp}^2}{r_s} \tilde{B}_b^{(4)} \end{aligned} \quad (3)$$

$$\begin{aligned} \frac{\eta}{\gamma} \tilde{B}_b^{(4)''} = & - \left[-\frac{(\gamma + ig'x)B^2}{\gamma \Gamma p} + \frac{(\mathbf{B} \cdot \nabla)^2}{\rho \gamma (\gamma + ig'x)} \right] \tilde{B}_b^{(4)} \\ & + \left[\frac{(\mathbf{B} \cdot \nabla)(B_z V_z')}{(\gamma + ig'x)} + \frac{(B^2)'}{B^2} \right] \xi_r^{(2)} \\ & - \left[-\frac{(\gamma + ig'x)(\mathbf{J} \cdot \mathbf{B})}{i \gamma k_{\perp} B \Gamma p} + \frac{(\mathbf{J} \cdot \mathbf{B})(\mathbf{B} \cdot \nabla)^2}{i \rho \gamma (\gamma + ig'x) k_{\perp} B^3} \right. \\ & \left. + \frac{(B_z V_z')}{\gamma B^2} \right] \tilde{B}_r^{(4)}, \end{aligned} \quad (4)$$

where equilibrium quantities are defined at the resonant surface, and $k_{\perp} B|_{r_s} = mB^2/r_s B_z$. The equations reduce to those of a slab [10–12] when the curvature [last term of Eq. (3)] is zero. We use the flow shear ordering for the parallel magnetic field and displacement,

$$\begin{aligned} \xi_r^{(2)} &= \xi_{r0}^{(2)} + iG' \xi_{rG}^{(2)} - G'^2 \xi_{rG}^{(2)} + \dots \\ \tilde{B}_b^{(4)} &= \tilde{B}_{b0}^{(4)} + iG' \tilde{B}_{bG}^{(4)} - G'^2 \tilde{B}_{bG}^{(4)} + \dots \end{aligned} \quad (5)$$

where $G' = (\eta r_s^3 / \Omega_R^6)^{1/5} g'$, $\Omega_R = (\eta m^2 q'^2 B_0^2 / \rho r_s^2 q^2)^{1/3}$, $\xi_{rG}^{(2)}$, and $\tilde{B}_{bG}^{(4)}$ are the first order solutions with flow shear. From this expansion, we obtain first order solutions at the low resistivity limit in terms of the zeroth order solutions (solutions without flow shear, expressible as a sum of Hermite functions) and we construct the axial Maxwell stress term [$\langle \tilde{J} \times \tilde{B} \rangle_z = (1/r) \langle r \tilde{B}_r \tilde{B}_z' \rangle$, where $\langle \rangle$ denotes flux surface averaged]. Note that the Lorentz force without flow vanishes due to a 90° phase shift between $\tilde{B}_{b0}^{(4)}$ and $\tilde{B}_r^{(4)}$.

Using the parallel displacement,

$$\begin{aligned} \xi_b^{(0)} = & \frac{1}{\rho \gamma (\gamma + ig'x)} \left[-\rho \gamma \xi_r^{(2)} \frac{(B_z V_z')}{B^2} \right. \\ & \left. + \frac{(\mathbf{B} \cdot \nabla)}{B^2} \left(B^2 \tilde{B}_b^{(4)} + \frac{(\mathbf{J} \cdot \mathbf{B})}{i(k_{\perp} B)} \tilde{B}_r^{(4)} \right) \right], \end{aligned} \quad (6)$$

we construct the Reynolds stress [$\langle \tilde{V} \cdot \nabla \tilde{V} \rangle_b = (\gamma^2/r) \times \langle r \xi_r^{(2)} \xi_b^{(0)'} \rangle$] using an expansion similar to Eq. (5). Expressing the first order solutions in terms of shear flow, the Lorentz force and the Reynolds stress are calculated for the inner layer region and shown in Fig. 1. The solutions are localized around resonant surface and radially integrate to zero. Thus, these structures transport momentum to reduce the flow gradient while conserving the total momentum in the plasma. The radial width is determined by the resistive layer width, unrelated to the width of the resulting magnetic island. It can be shown that both the Lorentz and fluid stress terms are small in the outer region. Therefore, momentum transport occurs mainly in the inner layer.

The approximate analytic quasilinear results are consistent with computational solution of the full MHD equations in the linear regime, which we perform using the DEBS code [15]. The equilibrium field and flow are chosen to be identical to those of the analytical calculations. Also equivalent to the analytic calculations, the computations are performed in the nonviscous regime, $P_m < 0.4S^{-2/5} \Delta^{6/5} F'^{-2/5} \rho^{1/5}$ [16], with $P_m = \nu/\eta = 0.01$, where ν and P_m are viscosity and the magnetic Prandtl number, respectively. Figure 2(a) shows the fluid stress term $\langle \tilde{V} \cdot \nabla \tilde{V} \rangle_z$ and Lorentz term $\langle \tilde{J} \times \tilde{B} \rangle_z$ during the linear growth phase. The stresses are localized and similar in

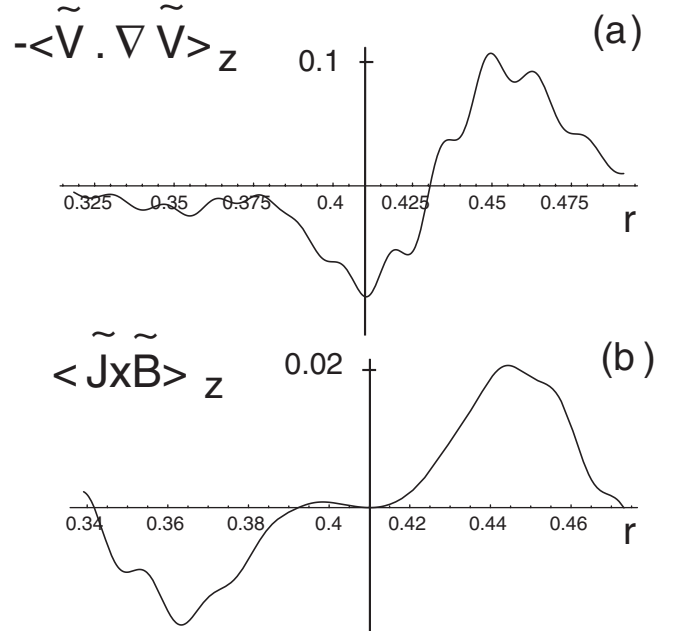


FIG. 1. The analytical quasilinear inner layer solutions for (a) the axial fluid stress $-\langle \tilde{V} \cdot \nabla \tilde{V} \rangle_z$ and (b) the axial Lorentz force $\langle \tilde{J} \times \tilde{B} \rangle_z$. The origin is the location of the resonant surface. The solutions are for the core tearing mode, $m = 1$ and $k_z = 2.0$, with an equilibrium current $\lambda = J_{\parallel}/B = \lambda_0(1 - r^\alpha)$ ($\lambda_0 = 3.2$ and $\alpha = 3$, $S = 10^4$, $\Delta' = 6.1$). The small oscillations are an artifact of the Hermite series truncation.

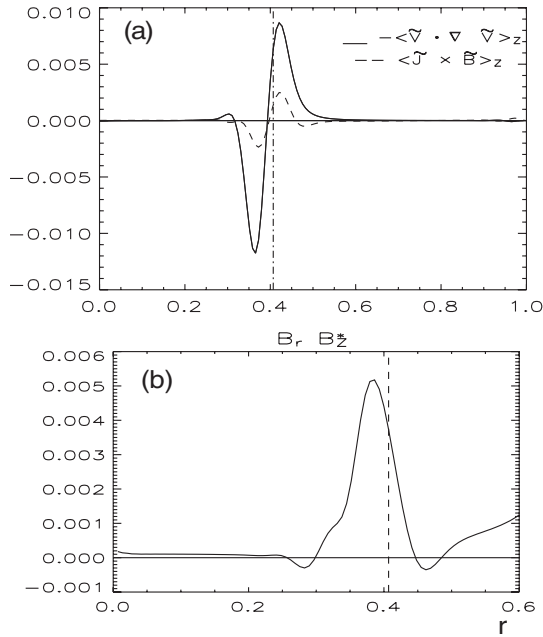


FIG. 2. (a) Axial fluid stress $-\langle \tilde{V} \cdot \nabla \tilde{V} \rangle_z$ and axial Lorentz force $\langle \tilde{J} \times \tilde{B} \rangle_z$ from linear single mode computations ($\rho = 1$); (b) radial structure of $\cos(\delta)$, where δ is the phase between \tilde{B}_r and \tilde{B}_z^* with $P_m = 0.01$ [$\langle \tilde{J} \times \tilde{B} \rangle_z = \frac{1}{r} [r |\tilde{B}_z| |\tilde{B}_r| \cos(\delta)]$]. The vertical line denotes the location of the resonant surface.

radial structures to the analytic solutions. Differences in detail likely arise from the constant ψ approximation of the analytics, not true for computation. Both computation and quasilinear calculations yield a fluid stress 5 times larger than the Maxwell stress [Figs. 1 and 2(a)]. The nonzero contribution of $\langle \tilde{J} \times \tilde{B} \rangle_z$ arises from the phase between \tilde{B}_r and \tilde{B}_z^* around the resonant surface [Fig. 2(b)].

To examine the nonlinear evolution of a single mode (as well as the multimode case), we again employ the DEBS code [15], but with an *ad hoc* momentum source $F(r)$ added to the momentum equation. The source is added to generate flow. The transport is then determined by plasma fluctuations. The effect of the forces on the flow during the nonlinear phase of a single mode computation with $P_m = 0.01$ is shown in Fig. 3. The flow profile is flattened around the resonant surface, as for the analytical calculations. The flow flattens very rapidly, in about 1000th of a viscous diffusion time (or 0.05 resistive diffusion times). Separate computation in which the flow is chosen to be dominantly perpendicular or dominantly parallel (to the equilibrium field) reveals that both flows are flattened similarly.

Computation with multiple tearing modes, as occurs in the RFP, reveals the additional effects of nonlinear mode coupling. The simulation is begun with $F(r) = 0$ (with $S = 5 \times 10^4$, $P_m = 10$, aspect ratio $R/a = 1.66$ and radial, azimuthal, and axial resolutions $n_r = 200$, $n_\theta = 16$, and $n_z = 128$, respectively). After reaching a quasistationary RFP state, $F(r)$ is switched on at $t/\tau_R = 0.085$ with a profile $F(r) = \text{const}$. The radial structure of the force is

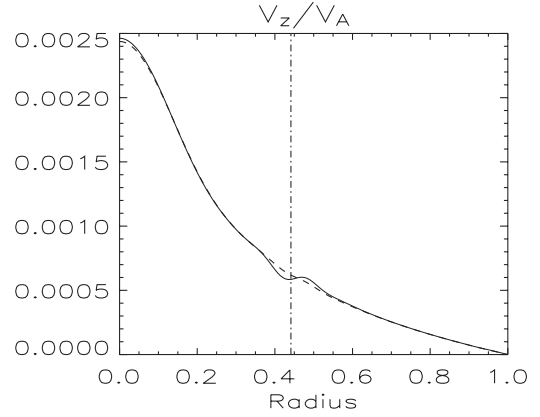


FIG. 3. Radial profile of axial flow (averaged over axial and azimuthal directions) for a single mode in its initial state (dashed line) and nonlinear state (solid line).

such that the axial flow profile would become parabolic in the absence of fluctuation-induced stresses. The tearing fluctuations undergo a repetitive sawtooth cycle, as shown in Fig. 4(a). After the force is applied the flow builds, saturating at $V_z = 0.06V_A$ [Fig. 4(b)]. However, the flow is strongly influenced by the sawtooth oscillations of the fluctuations. Flow profiles for two times, t_1 and t_2 , are shown in Fig. 4(b). As is seen, the flow becomes flatter in the core at time t_2 when fluctuations are large. The flattening arises from the Lorentz force from tearing fluctuations, shown in Fig. 5(a) for time t_2 . The Reynolds stress is small since the flow fluctuations are reduced by viscosity. The Lorentz force arises from multiple tearing modes, as shown in Fig. 5(b) for core-resonant $m = 1$ modes and the edge-resonant $m = 0$ mode.

The observed momentum transport is much more rapid than would occur without fluctuations. The time scale for flattening is about one-tenth of the viscous diffusion time. Moreover, this comparison understates the effect of the tearing stresses. To isolate the effect of the tearing modes,

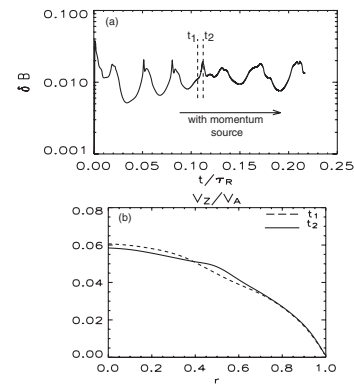


FIG. 4. (a) Total volume integrated magnetic fluctuations $\sqrt{1/2 \int B_r^2 dv}$ versus time. (b) Plasma flow profiles for times t_1 and t_2 .

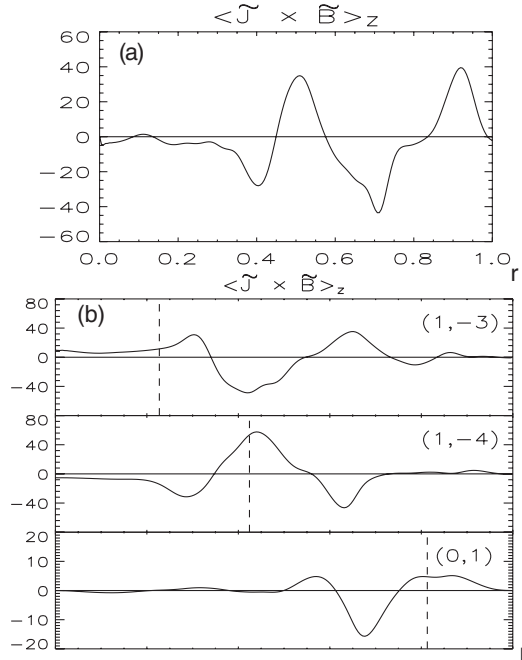


FIG. 5. Radial structure of (a) total $\langle \tilde{J} \times \tilde{B} \rangle_z$ force (summed over all n and m mode numbers), (b) $\langle \tilde{J} \times \tilde{B} \rangle_z$ force for a subset of individual modes [with $(m, n) = (1, -3), (1, -4), (0, 1)$] for time $t_2/\tau_R = 0.112$.

we have performed a computation in which the modes are turned off at t_1 , immediately before the onset of the momentum-flattening reconnection event. We observe that the flow profile *peaks* due to the modest dominance of the *ad hoc* force over viscous diffusion. Thus, the flattening dominantly occurs from the tearing stresses. The exception is the edge, where the torques localized at about $r/a \approx 0.92$ [Fig. 5(a)] are countered by viscous torques arising near the no-slip boundary. The radial width of the Lorentz forces is substantially larger than that of a single mode. Apparently, nonlinear coupling broadens the radial structures.

To clarify the effect of nonlinear coupling, we perform nonlinear computation in which the $m = 0$ mode is removed. It is known that the $m = 0$ mode mediates the coupling between $m = 1$ modes (with different n values). As a result, computation without $m = 0$ modes eliminates the dominant $m = 1$ mode coupling. The plasma evolves to a quasisteady state without sawtooth oscillations. The Lorentz force is reduced about fourfold across 80% of the plasma radius, and it becomes unidirectional in the core. Thus, the flattening of the flow profile does not occur (Fig. 6), and momentum transport is greatly reduced.

In summary, we have established theoretically that the Maxwell and Reynolds stresses arising from tearing instabilities can transport momentum rapidly in the RFP. In the presence of equilibrium flow, a single tearing mode can transport momentum much more rapidly than classical viscous forces, as established through quasilinear theory

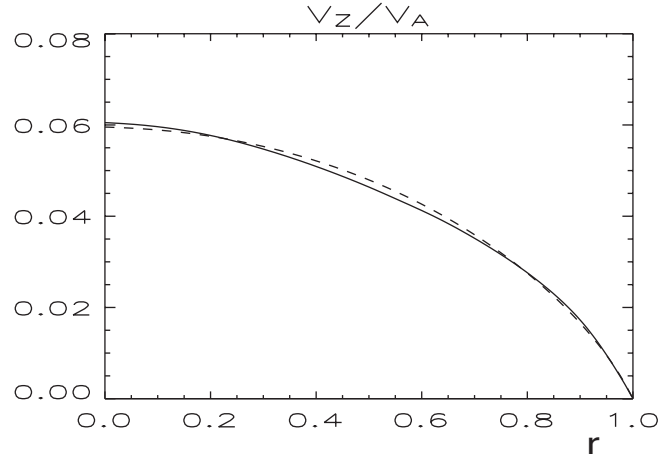


FIG. 6. Flow profiles without total fluctuations (dashed line) and without $m = 0$ modes (solid line).

and nonlinear MHD computation. Moreover, the inclusion of multiple tearing modes, resonant at different radii, substantially increases momentum transport. Nonlinear mode coupling amplifies the transport. Aspects of the theoretical results are consistent with experiment (such as the effect of nonlinear coupling on the phase shift between current and magnetic field fluctuations in the Maxwell stress). However, much of the theoretical predictions awaits experimental test. Future work will also investigate whether momentum transport by multiple current-driven reconnections might apply to astrophysical situations, perhaps complementing the well-developed model based on flow-driven instability.

-
- [1] A. K. Hansen *et al.*, Phys. Rev. Lett. **85**, 3408 (2000).
 - [2] S. A. Balbus and J. F. Hawley, Astrophys. J. **376**, 214 (1991).
 - [3] B. Coppi and P. S. Coppi, Phys. Rev. Lett. **87**, 051101 (2001).
 - [4] C. C. Hegna, Phys. Plasmas **3**, 4646 (1996).
 - [5] R. Fitzpatrick, Phys. Plasmas **6**, 1168 (1999).
 - [6] D. Dobrott, S. C. Prager, and J. B. Taylor, Phys. Fluids **20**, 1850 (1977).
 - [7] R. K. Pollard and J. B. Taylor, Phys. Fluids **22**, 126 (1979).
 - [8] R. Gatto, P. W. Terry, and C. C. Hegna, Nucl. Fusion **42**, 496 (2002).
 - [9] I. Hofmann, Plasma Phys. **17**, 143 (1975).
 - [10] R. B. Paris and W. N.-C. Sy, Phys. Fluids **26**, 2966 (1983).
 - [11] A. Bondeson and M. Persson, Phys. Fluids **29**, 2997 (1986).
 - [12] X. L. Chen and P. J. Morrison, Phys. Fluids B **2**, 495 (1990).
 - [13] J. M. Finn, Phys. Plasmas **2**, 4400 (1995).
 - [14] B. Coppi, J. M. Greene, and J. L. Johnson, Nucl. Fusion **6**, 101 (1966).
 - [15] D. D. Schnack *et al.*, J. Comput. Phys. **70**, 330 (1987).
 - [16] A. Bondeson and J. R. Sobel, Phys. Fluids **27**, 2028 (1984).